

### Impact of Cr(III) complexation with organic acid on its adsorption in silts and fine sands

Zi-xuan Zhang, Lin Wu, Xiang-ke Kong, Hui Li, Le Song, Ping Wang, Yan-yan Wang

Citation:

Zhang ZX, Wu L, Kong XK, *et al.* 2024. Impact of Cr(III) complexation with organic acid on its adsorption in silts and fine sands. *Journal of Groundwater Science and Engineering*, 12(4): 347-359.

View online: <https://doi.org/10.26599/JGSE.2024.9280026>

#### Articles you may be interested in

[Assessing the effectiveness of nanoscale zero-valent iron particles produced by green tea for Cr\(VI\)-contaminated groundwater remediation](#)

*Journal of Groundwater Science and Engineering*. 2023, 11(1): 55-67 <https://doi.org/10.26599/JGSE.2023.9280006>

[Experimental study on the velocity-dependent dispersion of the solute transport in different porous media](#)

*Journal of Groundwater Science and Engineering*. 2019, 7(2): 106-114 <https://doi.org/10.19637/j.cnki.2305-7068.2019.02.002>

[Research advances in non-Darcy flow in low permeability media](#)

*Journal of Groundwater Science and Engineering*. 2021, 9(1): 83-92 <https://doi.org/10.19637/j.cnki.2305-7068.2021.01.008>

[Transformation of ammonium nitrogen and response characteristics of nitrifying functional genes in tannery sludge contaminated soil](#)

*Journal of Groundwater Science and Engineering*. 2022, 10(3): 223-232 <https://doi.org/10.19637/j.cnki.2305-7068.2022.03.002>

[Effect of groundwater on the ecological water environment of typical inland lakes in the Inner Mongolian Plateau](#)

*Journal of Groundwater Science and Engineering*. 2022, 10(4): 353-366 <https://doi.org/10.19637/j.cnki.2305-7068.2022.04.004>

[Using pore-solid fractal dimension to estimate residual LNAPLs saturation in sandy aquifers: A column experiment](#)

*Journal of Groundwater Science and Engineering*. 2022, 10(1): 87-98 <https://doi.org/10.19637/j.cnki.2305-7068.2022.01.008>

## Research Article

## Impact of Cr(III) complexation with organic acid on its adsorption in silts and fine sands

Zi-xuan Zhang<sup>1,2,6</sup>, Lin Wu<sup>2,5</sup>, Xiang-ke Kong<sup>2,3,4\*</sup>, Hui Li<sup>2,4</sup>, Le Song<sup>2,4</sup>, Ping Wang<sup>3,4</sup>, Yan-yan Wang<sup>2,4</sup><sup>1</sup> School of Water Resources and Environment, China University of Geosciences (Beijing), Beijing 100083, China.<sup>2</sup> Key Laboratory of Groundwater Remediation of Hebei Province and China Geological Survey, Chinese Academy of Geological Sciences, Shijiazhuang 050061, China.<sup>3</sup> Fujian Provincial Key Laboratory of Water Cycling and Eco-Geological Processes, Xiamen 361021, Fujian, China.<sup>4</sup> Institute of Hydrogeology and Environmental Geology, Chinese Academy of Geological Sciences, Xiamen 361021, Fujian, China.<sup>5</sup> College of Water Resources, North China University of Water Resources and Electric Power, Zhengzhou 450046, China.<sup>6</sup> Shenzhen Geology Group Co. Ltd., Shenzhen 518000, Guangzhou, China.

**Abstract:** Trivalent chromium (Cr(III)) can form stable soluble complexes with organic components, altering its adsorption properties in the water-soil environment. This increases the risk of Cr(III) migrating to deeper soils and transforming into toxic Cr(VI) due to the presence of manganese oxides in sediments. In this study, Citric Acid (CA) was selected as a representative organic ligand to prepare and characterize Cr(III)-CA complexes. The characteristics, mechanisms and environmental factors influencing the adsorption of Cr(III)-CA on porous media (silts and fine sands) were investigated in the study. The results show that Cr(III) coordinates with CA at a 1:1 molar ratio, forming stable and soluble Cr(III)-CA complexes. Compared to Cr(III) ions, the equilibrium adsorption capacity of Cr(III)-CA is an order of magnitude lower in silts and fine sands. The adsorption of Cr(III)-CA in silts and fine sands is dominated by chemical adsorption of monolayers, following the pseudo-second-order kinetic equation and the Langmuir isotherm adsorption model. Varying contents of clay minerals and iron-aluminum oxides prove to be the main causes of differences in adsorption capacity of Cr(III)-CA in silts and fine sands. Changes in solution pH affect the adsorption rate and capacity of Cr(III)-CA by altering its ionic form. The adsorption process is irreversible and only minimally influenced by ionic strength, suggesting that inner-sphere complexation serves as the dominant Cr(III)-CA adsorption mechanism.

**Keywords:** Cr(III); Cr(III)-citric acid; Porous media; Adsorption; Inner-sphere complexation

Received: 20 Mar 2024/ Accepted: 17 Aug 2024/ Published: 06 Dec 2024

## Introduction

China is a major leather producer, accounting for approximately 21% of the world's total leather production annually. Despite the significant economic benefits of the leather industry, Cr-

induced environmental contamination requires more attention (Ma et al. 2017). Cr(III) salts are commonly used as tanning agents in the leather-making process (Zeng et al. 2016). Statistics indicate that about 1% to 4% of Cr(III) remains in wastewater and sludge during the leather-making process (Pantazopoulou et al. 2017; Reijonen et al. 2016). Although Cr(III) exhibits weak toxicity and low migration capability in soils, its accumulation and subsequent oxidation into Cr(VI) pose a significant environmental risk (Li et al. 2023; Manoj et al. 2021; Guo et al. 2020). During the tanning process, the addition of carboxylic acid and hydroxycarboxylic acid masking agents, along with the hydrolysis of skin collagen, allows partial Cr(III) to coordinate with organic components,

\*Corresponding author: Xiang-ke Kong, E-mail address: [kongxiangke@mail.cgs.gov.cn](mailto:kongxiangke@mail.cgs.gov.cn)

DOI: 10.26599/JGSE.2024.9280026

Zhang ZX, Wu L, Kong XK, et al. 2024. Impact of Cr(III) complexation with organic acid on its adsorption in silts and fine sands. Journal of Groundwater Science and Engineering, 12(4): 347-359.

2305-7068/© 2024 Journal of Groundwater Science and Engineering Editorial Office. This is an open access article under the CC BY-NC-ND license (<http://creativecommons.org/licenses/by-nc-nd/4.0>)

forming Cr(III) organic ligands at concentrations of about 2–10 mg/L in wastewater (Qiang et al. 2014; Dai et al. 2009). These Cr(III) organic ligands cannot be completely removed by conventional wastewater treatment methods, leading to further soil and groundwater contamination (Wang et al. 2016).

Cr(III)-organic complexes refer to the compounds formed through the coordination and complexation of Cr(III) with organic ligands. These complexes have a relatively stable structure, centered around Cr surrounded by saturated ligands (James and Bartlett, 1983; Hao et al. 2022). In natural soil environments, organic acids (like oxalic, citric, and malic acids) that contain active functional groups such as carboxyl and phenolic hydroxyl groups, can coordinate with Cr(III) to form stable compounds (Merdoud et al. 2016; Kanagaraj et al. 2019; Tripathi et al. 2020). Compared to inorganic Cr(III), Cr(III)-organic complexes demonstrate significantly enhanced solubility and stability in water-soil environments, greatly influencing the forms of Cr(III) in soils, as well as their migration and transformation (Puzon et al. 2008; Gustafsson et al. 2014). Researches have shown that Cr(III) and Cr(VI) are commonly detected in deep soils and groundwater around tanneries (Sethunathan et al. 2005; Shashirekha et al. 2015; Kong et al. 2020).

Adsorption plays a pivotal role in determining the migration of metal-organic complexes in water-soil environments (Schwab et al. 2005). Cr(III)-organic complexes occur in significantly different forms under varying pH values (Dai et al. 2009). The adsorption of these complexes is subjected to the physicochemical properties of porous media and environmental factors (Li et al. 2022). Some researchers have conducted comparative analyses of the adsorption capacities of nine Cr(III)-organic complexes in soils, revealing that the principal mechanisms influencing the adsorption include electrostatic attraction, hydrogen bonding, and inner-sphere complexation (Luo et al. 2010). Other studies have explored the adsorption processes of Cr(III)-CA and Cr(III)-EDTA in yellowish-brown, red, and black soils, suggesting that free radicals in soils may be the primary cause of specific adsorption (Cao et al. 2011). However, previous researches have mostly focused on the adsorption and migration behaviors of Cr(III)-organic complexes in different types of soils. There is a lack of systematical analyses of the adsorption patterns of Cr(III)-organic complexes on porous media and the influence of environmental factors on adsorp-

tion. This gap limits the understanding of the potential environmental risks posed by Cr(III)-organic complexes.

The Xinji leather industrial zone in Hebei Province is the largest leather production, trading, and processing base in North China. It is situated in the alluvial-proluvial fan area of the Hutuo River, where the vadose zone is composed primarily of silts and fine sands. Due to the complex process and high costs associated with tannery wastewater treatment, some enterprises frequently discharge substandard Cr-containing wastewater, posing enormous risks of environmental contamination (Kong et al. 2019). In this study, Citric Acid (CA), which is ubiquitous in natural environments and leather industrial production, is selected as a representative organic ligand. Based on the preparation and qualitative characterization of Cr(III)-CA complexes, the kinetic and thermodynamic characteristics, as well as the environmental factors influencing Cr(III)-CA adsorption in typical porous media (silts and fine sands) in the vadose zone are explored. The study reveals the mechanism and environmental factors influencing Cr(III)-CA adsorption on porous media, aiming to provide theoretical support for research on both the migration behavior of Cr(III)-organic complexes on porous media and for the risk assessment of Cr contamination.

## 1 Materials and methodology

### 1.1 Experimental materials

The experimental reagents used in this study included Citric Acid (CA) and chromium chloride hexahydrate ( $\text{CrCl}_3 \cdot 6\text{H}_2\text{O}$ ), both purchased from Tianjin Kaitong Reagent Co., Ltd. Methanol, ethanol, and acetone, all chromatographic reagents, were purchased from MREDA Technology Inc. Sodium hydroxide (NaOH) and hydrochloric acid (HCl) were obtained from Aladdin and Beijing Chemical Works, respectively. All experimental reagents were of analytical or guaranteed reagents, and ultrapure water was used throughout the experiments.

The porous media used in this study are silts and fine sands collected from the alluvial-proluvial fan area of the Hutuo River in Shijiazhuang City. Before the experiments, the silts and fine sands were sieved to 100 mesh and 40–60 mesh, respectively, to remove residues and plant roots. They were then sterilized three times using high-pressure steam sterilization at 120°C and then kept

sealed for later use. Mineral test results indicated that the fine sands were primarily composed of feldspar and quartz, accounting for 67.1% and 31.0% of the total physical phase, respectively. In contrast, the silts principally comprised quartz, feldspar, montmorillonite, and chlorite, representing 36.9%, 24.8%, 10.7%, and 9.1% of the total physical phase, respectively. The general physico-chemical properties of the two porous media are shown in Table 1.

## 1.2 Preparation of Cr(III)-CA

The preparation method for Cr(III)-CA was optimized based on previous literature (Li, 2009). At room temperature ( $25\pm 2^\circ\text{C}$ ), 4.80 g of CA and 6.66 g of  $\text{CrCl}_3\cdot 6\text{H}_2\text{O}$  were weighed and placed into a 250 mL beaker, to which 100 mL of ultrapure water was added to completely dissolve the solids while stirring. The pH of the solution was adjusted to 4.0–5.0 using 2.0 mol/L NaOH. Subsequently, the solution was transferred to a three-neck flask, and heated to  $80^\circ\text{C}$  while stirring for 8 h. After the reaction solution cooled down to room temperature, blueish-purple precipitates appeared. These precipitates were extracted by filtration and washed several times with anhydrous ethanol. The collected precipitates were then freeze-dried in a vacuum, yielding Cr(III)-CA powders, which were then stored in a dry and dark place for future use.

## 1.3 Experimental methodology

### 1.3.1 Adsorption kinetics experiments

Certain amounts of  $\text{CrCl}_3\cdot 6\text{H}_2\text{O}$  and Cr(III)-CA prepared were weighed. Using a 0.01 mol/L NaCl background solution,  $\text{CrCl}_3\cdot 6\text{H}_2\text{O}$  and Cr(III)-CA were used to prepare Cr(III)-CA and Cr(III) solutions with initial Cr(III) concentrations of 2.5 mg/L, 11.0 mg/L, and 26.0 mg/L. Subsequently, 1.0 g of fine sands and 1.0 g of silts were weighed and placed into 40 mL brown bottles. Next, 10.0 mL of the Cr(III)-CA and Cr(III) solutions were pipetted into the brown bottles, which were then sealed and placed in a shaker to be agitated in the dark at  $25^\circ\text{C}$  and 150 rpm. Samples from these solutions were collected and tested at intervals of

10 min, 20 min, 30 min, 1 h, 2 h, 4 h, 6 h, 8 h, 12 h, 24 h, and 48 h.

### 1.3.2 Isothermal adsorption and desorption experiments

A certain amount of Cr(III)-CA was weighed. Then Cr(III)-CA and 0.01 mol/L NaCl background solution were used to prepare the Cr(III)-CA solutions with initial Cr(III) concentrations of 2.5 mg/L, 5.0 mg/L, 7.5 mg/L, 10.0 mg/L, 15.0 mg/L, 20.0 mg/L, 40.0 mg/L, 60.0 mg/L, 80.0 mg/L, and 100.0 mg/L. Subsequently, 2.0 g of fine sands and 2.0 g of silts were accurately weighed and placed in separate 40 mL brown bottles. Cr(III)-CA solutions with various concentrations (20.0 mL each) were pipetted into the brown bottles, which were sealed and placed in a shaker for agitation in the dark at  $25^\circ\text{C}$  and 150 rpm. After 48 hours, the solutions were sampled for testing to determine reaction equilibrium.

Desorption experiments were then conducted. After reaching adsorption equilibrium, the reaction solutions were removed from the bottles. Subsequently, 10.0 mL of 0.01 mol/L NaCl solution was added to each bottle, which were sealed and placed in a shaker for agitation in the dark at  $25^\circ\text{C}$  and 150 rpm. After 48 hours, the reaction solutions were sampled for testing.

### 1.3.3 Experiments on the impacts of environmental factors

**Impacts of pH:** 2.0 g of fine sands and 1.0 g of silts were weighed and placed into separate 40 mL brown bottles. To each bottle, 20.0 mL of Cr(III)-CA solutions with pH values ranging from 2.0 to 11.0 and a Cr(III) concentration of 14.0 mg/L were added. The brown bottles were then sealed and placed in a shaker for agitation in the dark at  $25^\circ\text{C}$  and 150 rpm. After 48 hours, the reaction solutions were sampled for testing.

**Impacts of ionic strength and coexisting cations:** Cr(III)-CA solutions with a Cr(III) concentration of 14.0 mg/L were prepared by merely changing the background solution. Specifically, solutions of KCl,  $\text{CaCl}_2$ , and  $\text{MgCl}_2$  with concentrations of 0.001 mol/L, 0.01 mol/L and 0.1 mol/L were individually used as background solutions. Subsequently, experiments on Cr(III)-CA adsorption in silts were conducted. The subse-

**Table 1** Physical and chemical properties of the experimental soils

Porous media	TOC (g/kg)	pH	CEC (cmol/kg)	$\text{Fe}_2\text{O}_3$ (%)	Ratio of particle size (%)		
					0–2 $\mu\text{m}$	2–20 $\mu\text{m}$	20–100 $\mu\text{m}$
Silts	8.5	8.22	6.8	6.13	10.52	74.39	15.09
Fine sands	7.2	7.52	5.6	3.48	1.07	7.28	91.65

quent reaction conditions and operating procedures were identical to those of isothermal adsorption experiments.

**Impacts of iron-aluminum oxides:** Iron-aluminum oxides were prepared using the precipitation method. Specifically, a mixed solution with a concentration of 1.0 mol/L was prepared by mixing  $\text{FeCl}_3$  and  $\text{AlCl}_3$  at a molar ratio of 1:1. Under magnetic stirring, the pH of the solution was adjusted to 7.4 by slowly adding 3.0 mol/L NaOH. After further stirring for 30 min, the reaction product was collected and aged at 60°C for 24 hours. The precipitates were obtained through centrifugation, rinsed several times with deionized water, and finally freeze-dried in a vacuum, yielding iron-aluminum oxide samples. Additionally, the prepared iron-aluminum oxides were added to silts or fine sands at mass ratios of 0.5 wt%, 1 wt%, 5 wt%, and 10 wt%. After thorough mixing, the mixtures were added to 20 mL of Cr(III)-CA solution with a concentration of 12.4 mg/L. The subsequent reaction conditions and operating procedures were identical to those of isothermal adsorption experiments.

In each experiment, two duplicate samples and one control sample were retained. Concentration tests of Cr(III) and Cr(VI) in the control samples revealed negligible loss of Cr(III) in solutions due to adsorption on containers and precipitation during reactions (< 1 wt%), with Cr(VI) undetected (< 0.005 mg/L).

## 1.4 Analytical methods

### 1.4.1 Testing methods

To conduct testing, 0.25 g of  $\text{CrCl}_3 \cdot 6\text{H}_2\text{O}$  and 0.25 g of Cr(III)-CA were weighed and dissolved to obtain a 100 mL solution, respectively. The ultraviolet-visible absorption spectrum of the solution was obtained using a UV-2550 ultraviolet spectrophotometer supplied by Shimadzu, Japan. Scanning was performed within a range of 190–700 nm at a scanning speed of 500 nm/min and resolution of 0.02 nm. Furthermore, 0.05 g of solid Cr(III)-CA was weighed and dissolved in pure water to determine the concentrations of Cr and Total Organic Carbon (TOC) in the solution. The theoretical contents of Cr and C elements in Cr(III)-CA were calculated based on the element mass ratios. Additionally, certain amounts of dry CA, Cr(III)-CA powders, and potassium bromide were mixed, ground, and pressed into a tablet. The infrared spectrum of the tablet was obtained by scanning within a range of 400–4000  $\text{cm}^{-1}$  using a Nicolet 6700 infrared spectrometer from Thermo Fisher, USA.

Prior to experiments, solution samples were filtered using 0.22  $\mu\text{m}$  organic membrane filters. The total Cr, K, Na, and Mg concentrations were determined using an Optima 8000 inductively coupled plasma emission spectrometer supplied by PerkinElmer, USA. The TOC concentrations were determined using a TOC-L CPH analyzer from Shimadzu, Japan and the Cr(VI) was determined using the spectrophotometric method with 1,5-Diphenylcarbohydrazide, respectively. The Cr(III) concentration was calculated by subtracting the Cr(VI) concentration from the total Cr concentration.

### 1.4.2 Mathematical model analysis

The adsorption capacity of Cr(III)-CA and Cr(III) by porous media is calculated using Equation (1) (Zhang et al. 2022):

$$C_s = (C_0 - C_e) \cdot V/m \quad (1)$$

Where:  $C_s$  is the solid-phase adsorbed amount ( $\mu\text{g/g}$ ),  $C_0$  is the initial concentration of contaminant ( $\mu\text{g/L}$ ),  $C_e$  is the liquid phase concentration at equilibrium ( $\mu\text{g/L}$ ),  $V$  is solution volume (mL),  $m$  is the mass of added porous media (g).

The classical Lagergren pseudo-first order (Eq.(2)), pseudo-second-order kinetic (Eq. (3)) and Elovich models (Eq. (4)) were employed to fit the adsorption curves (Wang et al. 2022).

$$\log(Q_e - Q_t) = \log Q_e - k_1 \cdot \frac{t}{2.203} \quad (2)$$

$$\frac{t}{Q_t} = \frac{1}{k_2} \cdot Q_e^2 + \frac{t}{Q_e} \quad (3)$$

$$Q_t = \frac{1}{b} \cdot [\ln(ab) + \ln t] \quad (4)$$

Where:  $Q_e$  and  $Q_t$  are the adsorption capacities ( $\mu\text{g/g}$ ) at equilibrium and at time  $t$  (min), respectively.  $k_1$  is the equilibrium rate constant ( $\text{min}^{-1}$ ).  $k_2$  is the pseudo-second-order rate constant ( $\mu\text{g}/(\text{g} \cdot \text{min})$ ).  $a$  is the initial adsorption rate ( $\mu\text{g}/(\text{g} \cdot \text{h})$ ).  $b$  is the chemisorption activation energy parameters (g/mg).

The Freundlich (Eq.(5)) and Langmuir (Eq.(6)) adsorption isotherms are used to model the equilibrium adsorption data (Wang et al. 2013).

$$C_s = K_F \cdot C_e^n \quad (5)$$

$$C_s = Q_{max} \cdot K_L \cdot \frac{C_e}{1 + K_L \cdot C_e} \quad (6)$$

Where:  $K_F$  is the Freundlich constant ( $(\mu\text{g/g}) \cdot (\text{L}/\mu\text{g})^n$ ).  $n$  is an empirical exponent (the value range from 0 to 1).  $Q_{max}$  is the maximum adsorption capacity ( $\mu\text{g/g}$ ).  $K_L$  is the adsorption energy coefficient of Langmuir.

## 2 Results and discussion

### 2.1 Physicochemical properties of Cr(III)-CA

When Cr occurs as a complex in solution, its electrons undergo a transition from low-energy *d* orbitals to high-energy *d* orbitals. As observed in the ultraviolet-visible adsorption spectrum (Fig. 1a), two maximum adsorption peaks of CrCl<sub>3</sub> appeared at 427 nm and 612 nm. This phenomenon occurs due to the formation of a ligand field as interactions between Cr(III) and H<sub>2</sub>O take place. After the formation of complexes between Cr(III) and CA, the adsorption peaks shifted to 412 nm and 568 nm, respectively, with reduced wavelengths. This shift suggests a stronger ligand field and higher *d*-orbital splitting energy of Cr(III)-CA. A further comparison of the adsorption peaks between Cr(III)-CA and CA in the Fourier Transform Infrared (FTIR) spectrum (Fig. 1b) reveals that CA contains groups like -OH (3,295 cm<sup>-1</sup> and 3,497 cm<sup>-1</sup>), C=O (1,744 cm<sup>-1</sup>), -C-O (1,429 cm<sup>-1</sup>), and =C-H (781 cm<sup>-1</sup>). Upon coordination with Cr(III), some adsorption peaks in Cr(III)-CA experience shifting, enhancement, attenuation, or the formation of new peaks. For instance, the enhanced -OH adsorption peak appeared at 3,439 cm<sup>-1</sup>, while the adsorption peaks of C=O, -C-O, and =C-H shifted to 1,606 cm<sup>-1</sup>, 1,390 cm<sup>-1</sup>, and 860 cm<sup>-1</sup>, respectively, indicating that Cr(III) in solutions may coordinate with functional groups such as carboxyl and hydroxyl groups in CA. The C and Cr contents in Cr(III)-CA were further determined, revealing that their measured values (23.3% for C and 17.4% for Cr) approached their calculated values (23.0% for C and 17.2% for Cr), demonstrating that Cr(III) and CA coordinated at a

molar ratio of 1:1 produced stable Cr(III)-CA complexes, which is consistent with previous studies (Dai et al. 2009).

### 2.2 Adsorption kinetics

As shown in Fig. 2, the adsorption kinetics curves of Cr(III) and Cr(III)-CA on porous media indicate that Cr(III) exhibited high adsorption rates and capacities in both silts and fine sands, while Cr(III)-CA demonstrated low adsorption rates and capacities in them, specifically in fine sands. The adsorption capacity of Cr(III)-CA on porous media decreased by approximately one order of magnitude compared to that of Cr(III). In fine sands, the adsorption rates of Cr(III) with three distinct initial concentrations reached above 99.3% (Fig. 2a), while that of Cr(III)-CA remained below 26.5% (Fig. 2b). This discrepancy can be attributed to the pH buffering capacity of the porous media, leading to a swift increase in the pH of reaction solutions from 3.0 to 7.5. Consequently, the removal of Cr(III) was subjected to the combined effect of adsorption and precipitation on porous media. Compared to Cr(III) ions, Cr(III)-CA predominantly occurs as zwitterion ([Cr(III)-CA]<sup>±</sup>) in solutions with pH between 5.0 and 8.0, making it less prone to adsorption (Dai et al. 2009). Hence, Cr(III)-CA exhibits high solubility and stability in the solution, enhancing its migration capacity in porous media.

According to the fitting results of different dynamic models (Fig. 3, Table 2), the adsorption data of Cr(III)-CA with various concentrations on porous media were more effectively fitted by the pseudo-second-order kinetic equation ( $R^2 > 0.95$ ). Moreover, the fitted values ( $Q_{e,exp}$ ) were much closer to the measured values ( $Q_{e,cal}$ ), suggesting

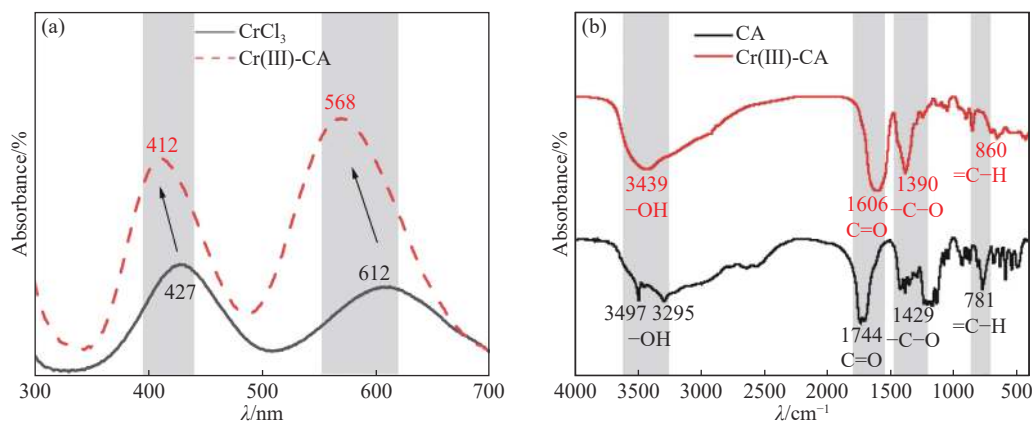


**Fig. 1** Comparative analysis of spectral responses of Cr(III) and Cr(III)-CA

(a: UV-vis, b: FTIR)

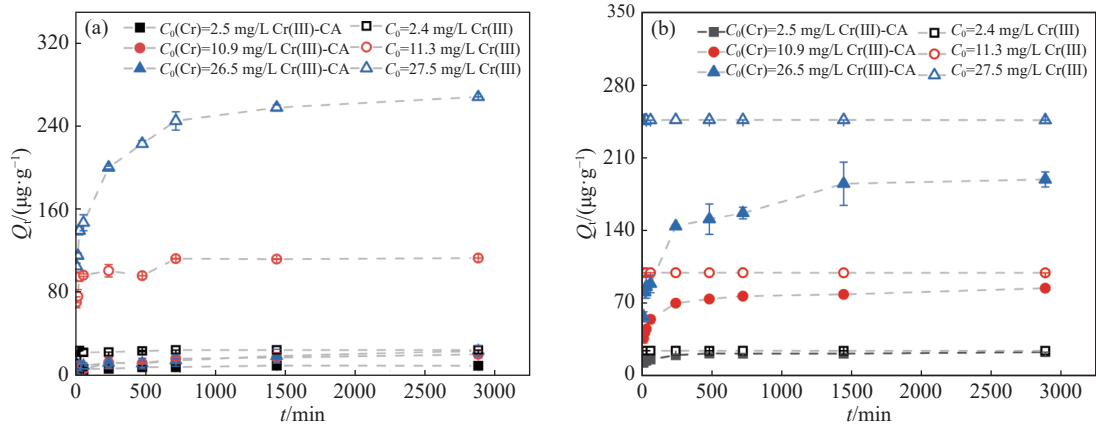


Fig. 2 Sorption of Cr(III) and Cr(III)-CA on porous media (a: Silts; b: Fine sands)

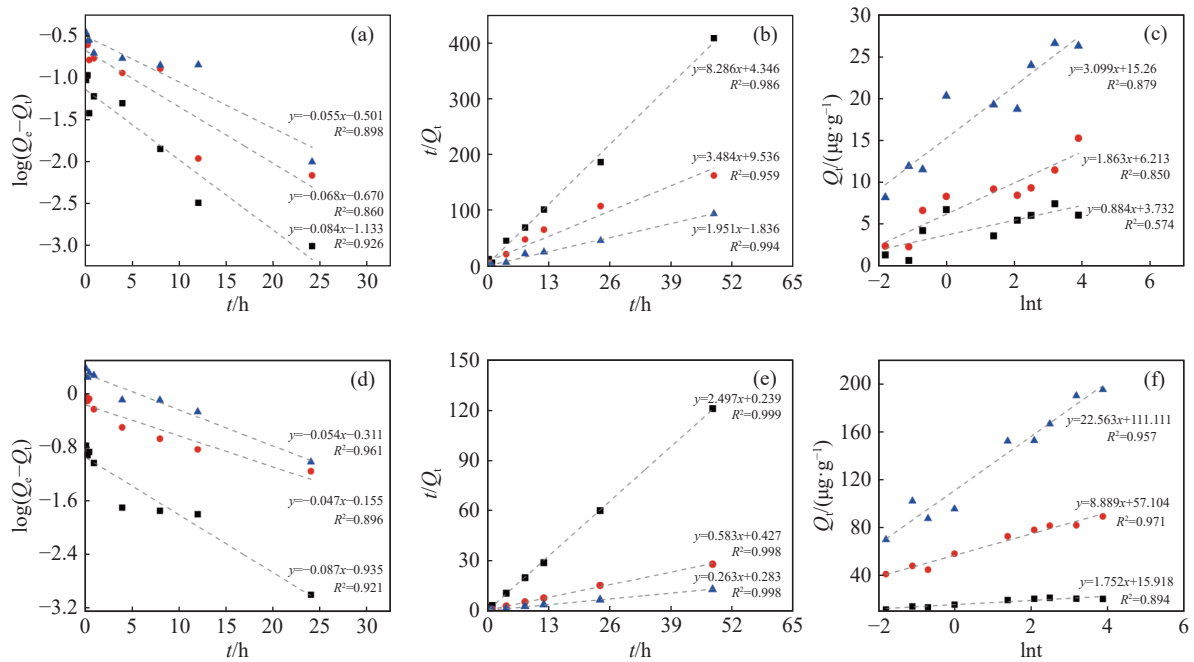


Fig. 3 Adsorption kinetics fitting results of Cr(III)-CA on porous media

Notes: (Fine sand: a, Pseudo first-order; b, Pseudo first-order; c, Elvovich. silt; d, Pseudo first-order; e, Pseudo first-order; f, Elvovich. ■:  $C_0$  2.5 mg/L; ●:  $C_0$  10.9 mg/L; ▲:  $C_0$  26.5 mg/L)

Table 2 Fitting parameters of Pseudo-second-order kinetic model for Cr(III)-CA adsorption

Porous media	Fine sands			Silts		
	$C_0$ (mg/L)	$Q_{e,exp}$ (µg/g)	$Q_{e,cal}$ (µg/g)	$K_2$ (g·h/µg)	$R^2$	
$C_0$ (mg/L)	2.50	10.90	26.50	2.50	10.90	26.50
$Q_{e,exp}$ (µg/g)	9.36	15.08	26.00	20.80	89.43	194.99
$Q_{e,cal}$ (µg/g)	6.24	14.04	26.00	20.80	87.87	193.43
$K_2$ (g·h/µg)	0.16	0.07	0.04	0.05	0.01	0.01
$R^2$	0.986	0.959	0.994	0.999	0.998	0.998

that the adsorption of Cr(III)-CA on porous media was predominantly achieved by chemical reactions. The adsorption capacity of Cr(III)-CA on porous media increased significantly with an increase in its initial concentration. As the initial concentration of Cr(III)-CA rose from 2.50 mg/L

to 26.50 mg/L, its equilibrium adsorption capacity in fine sands and silts increased from 6.24 µg/g to 26.00 µg/g and from 20.80 µg/g to 193.43 µg/g, respectively. Furthermore, the adsorption rate and equilibrium adsorption capacity of Cr (III)-CA in silts were significantly higher than those in fine

sands, possibly due to soil physical and chemical properties, such as phase composition, particle size, and Specific Surface Areas (SSAs) (Table 1).

### 2.3 Isotherm adsorption

The fitting results derived from the isothermal adsorption models (Fig. 4, Table 3) indicate that the adsorption data of Cr(III)-CA on porous media were well fitted by both Langmuir and Freundlich models, especially the Langmuir model. Notably, silts and fine sands manifested significant differences in the equilibrium adsorption capacity of Cr(III)-CA under the same initial concentrations. According to the Freundlich model, Cr(III)-CA experienced weak adsorption ( $n = 0.31-0.43$ ) on porous media, with silts demonstrating a much higher adsorption affinity coefficient ( $K_f$ ) for Cr(III)-CA than fine sands. Moreover, the Langmuir model revealed that the maximum adsorption capacity ( $Q_{max}$ ) of Cr(III)-CA in silts was 296.11  $\mu\text{g/g}$ , far exceeding that in fine sands (30.27  $\mu\text{g/g}$ ). This suggests that the adsorption affinity of Cr(III)-CA in silts is much higher than that in fine sands. Since silts have relatively large SSAs and high contents of clay minerals and organic matter (Table 1), they can provide more active adsorption sites, which enhances the adsorption of Cr(III)-CA. Although the adsorption isotherms of Cr(III)-CA in silts and fine sands exhibited relatively serious nonlinearity, they displayed linear adsorption (Fig.

4) in both media at low initial concentrations (2.5–10.0  $\text{mg/L}$ ). This indicates that the Cr(III)-CA adsorption process is significantly influenced by the distribution of organic ligand CA under low concentrations.

Under experimental pH (6.9–7.1), Cr(III)-CA primarily occurs as  $[\text{Cr(III)-CA}]^{\pm}$ . The desorption curves of Cr(III)-CA in silts and fine sands (Fig. 5) illustrate that the desorption concentration data points under different initial concentrations were all distributed below the 1:1 line representing the  $C_e$  to  $C_0$  ratio. This observation suggests that almost no desorption occurred for the adsorbed Cr(III)-CA. Thus, the adsorption of Cr(III)-CA on porous media is irreversible (Luo et al. 2010). The strong bonding force among active groups during the inner-sphere complexation leads to difficult desorption of the adsorbed substances. Therefore, inner-sphere complexation might serve as the dominant adsorption mechanism of Cr(III)-CA on porous media.

### 2.4 Adsorption mechanisms

#### 2.4.1 Impacts of physicochemical properties of porous media

The physicochemical properties of porous media exert a great influence on the adsorption mechanisms. To identify the impacts of soil properties on Cr(III)-CA adsorption, the adsorption isotherm

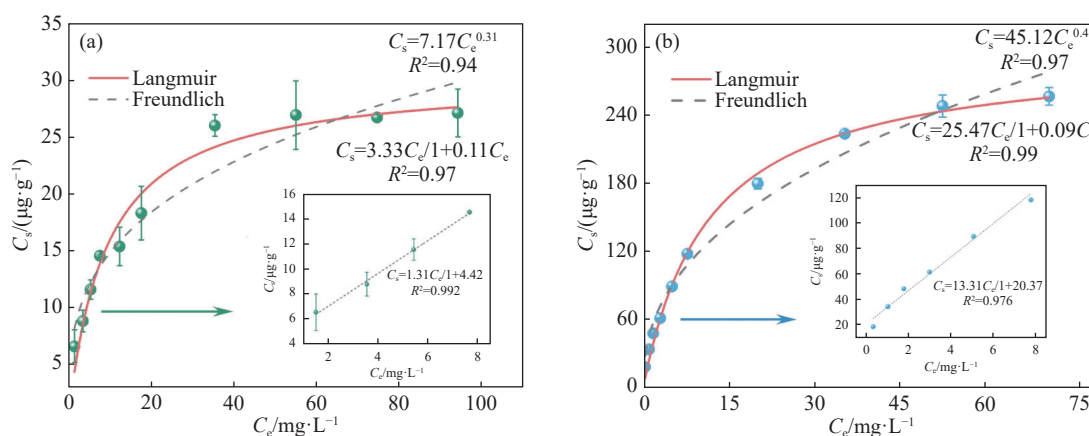
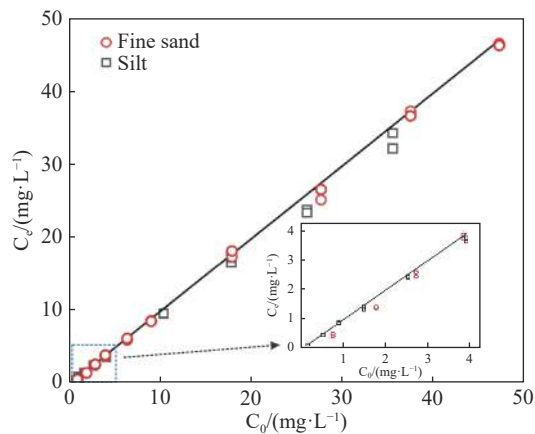


Fig. 4 Isothermal adsorption fitting results of Cr(III)-CA on porous media

(a: Fine sands; b: Silts)

Table 3 Fitting parameters of isothermal adsorption models for Cr(III)-CA adsorption

Porous media	Freundlich			Langmuir		
	$K_f [(\mu\text{g/g}) \cdot (\text{L}/\mu\text{g})^n]$	$n$	$R^2$	$Q_{max} (\mu\text{g/g})$	$K_L (\text{L}/\mu\text{g})$	$R^2$
Fine sands	7.17	0.31	0.94	30.27	0.09	0.97
Silts	45.12	0.43	0.98	296.11	0.11	0.99



**Fig. 5** Comparison of Cr(III)-CA concentration before and after desorption

data were normalized based on SSAs (Fig. 6). The SSAs of silts and fine sands were measured at 0.99 m<sup>2</sup>/g and 18.05 m<sup>2</sup>/g, respectively. However, under different concentration conditions, the adsorption capacity per unit SSAs of Cr(III)-CA in fine sands surpassed that in silts, suggesting that polarity contributed significantly to the adsorption of Cr(III)-CA on porous media (Shi et al. 2023).

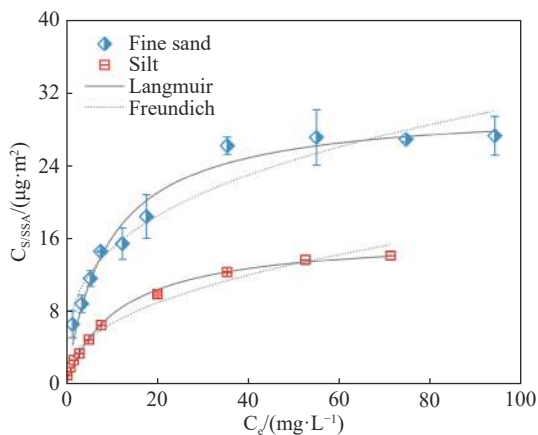


**Fig. 6** Specific surface areas-normalized sorption isotherms of Cr(III)-CA on porous media

Under experimental conditions, the organic matter contents in both silts and fine sands were relatively similar and low. However, despite this similarity, the adsorption capacity of Cr(III)-CA in silts was 9.8 times greater than that in fine sands. This phenomenon aligns with findings from previous studies (Cao et al. 2011), where the equilibrium adsorption capacities of Cr(III)-CA increased from 0.91 µmol/g to 1.22 µmol/g, from 1.64 µmol/g to 2.24 µmol/g, and from 2.92 µmol/g to 3.18 µmol/g in black, yellow, and red soils where organic matter is removed. Therefore, a decrease in organic matter content in soils promotes the adsorption of Cr(III)-CA. Hence, it is inferred that

the organic matter content on porous media is a minor factor affecting the Cr(III)-CA adsorption. Further comparison of mineral phase compositions in fine sands and silts, fine sands reveals notable differences. Fine sands exhibited a much higher proportion (67.1%) of feldspar minerals compared to silts (24.8%). Conversely, the proportion of clay minerals, including montmorillonite, illite, and chlorite, in silts was 7.2 times higher than that in fine sands. While feldspar minerals may contribute to weak electrostatic adsorption and ion exchange of Si-OH and Al-OH (Hizal et al. 2013), they are not likely the primary sites for Cr(III)-CA adsorption on porous media. Instead, clay minerals, characterized by their permanent and variable charges, play a more significant role. Cr(III)-CA can be absorbed on the surfaces of layered clay minerals like montmorillonite and illite through electrostatic attraction (Yang et al. 2022). Furthermore, Cr(III) in Cr(III)-CA may act as a metal bridge, forming a Fe-Cr(III)-CA ternary system with iron oxides containing functional groups like -OH<sup>-</sup>, -OH<sub>2</sub><sup>+</sup>, and -O<sup>-</sup> (Chiavola et al. 2019). Additionally, iron oxides coated on the surfaces of clay minerals, as the most critical and active inorganic component in soils, may undergo inner-sphere complexation with active groups like -COOH and -OH in Cr(III)-CA (Gérard, 2016). Therefore, the observed difference in the Cr(III)-CA adsorption capacity between silts and fine sands may result from variations in mineral types and iron oxide contents.

#### 2.4.2 Impacts of pH

The pH of a solution can significantly influence the adsorption process of Cr(III)-CA by altering its chemical form and the surface charges of the porous media (Kah et al. 2017). As shown in Fig. 7a-7b, the adsorption process of Cr(III)-CA on porous media can be divided into two phases: Rapid adsorption (0–4 h) and slow adsorption (4–48 h). With an increase in pH, both the adsorption rate and capacity of Cr(III)-CA gradually decreased in both fine sands and silts. Specifically, as the pH increased from 3.0 to 9.0, the initial adsorption rates of Cr(III)-CA in fine sands and silts decreased from 4.54 µg/g·h to 0.79 µg/g·h and from 12.24 µg/g·h to 10.20 µg/g·h, respectively. Notably, fine sands exhibited a weak pH buffering effect compared to silts. Consequently, variations in pH exerted a more pronounced influence on the adsorption of Cr(III)-CA in fine sands.

The distributions of Cr(III)-CA forms in solutions with varying pH solutions can be calculated (Dai et al. 2009). As shown in Fig. 7c, at pH 3.0,

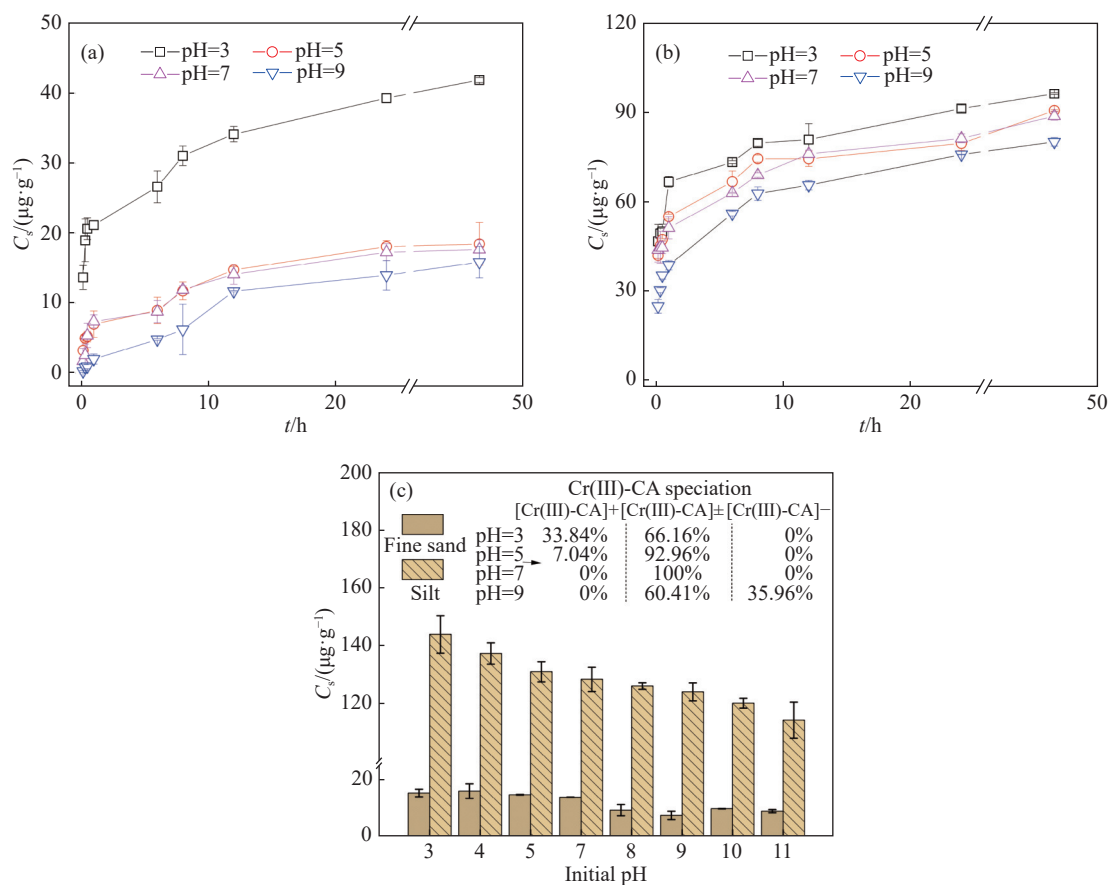


**Fig. 7** Changes of Cr(III)-CA adsorption on porous media at various pH

Notes: a: Adsorption curve on fine sands; b: Adsorption curve on silts; c: Adsorption capacity varies with pH

$[\text{Cr(III)-H-CA}]^+$ , carrying positive charges, accounted for 33.8% of Cr(III)-CA, with the remaining portion occurring as  $[\text{Cr(III)-CA}]^\pm$ . Between pH 5.0–8.0, Cr(III)-CA occurred predominantly as  $[\text{Cr(III)-CA}]^\pm$ , comprising nearly 93.0% of the total distribution. As the pH exceeded 9.0, Cr(III)-CA was dominated by  $[\text{Cr(III)-OH-CA}]^-$ , with the proportion of  $[\text{Cr(III)-CA}]^\pm$  diminishing. Therefore, as the initial pH increased from 3.0 to 11.0, the equilibrium adsorption capacity of Cr(III)-CA gradually decreased in fine sands and silts. At pH below 5.0, the Cr(III)-CA adsorption on porous media occurs primarily through the electrostatic adsorption and cation exchange of  $[\text{Cr(III)-H-CA}]^+$ , facilitated by the negative charges present on the porous media. In the pH range of 5.0–8.0, Cr(III)-CA predominantly exists as  $[\text{Cr(III)-H-CA}]^\pm$ , resulting in minor differences in adsorption on porous media. However, as the pH rises above 9.0, the increasing proportion of  $[\text{Cr(III)-OH-CA}]^-$  leads to a significant decrease in adsorption capacity due to electrostatic repulsion between  $[\text{Cr(III)-OH-CA}]^-$  and negatively charged porous media. The adsorption affinity of Cr(III)-CA with different valencies forms on porous media decreases in

the order of  $[\text{Cr(III)-H-CA}]^+$ ,  $[\text{Cr(III)-CA}]^\pm$ , and  $[\text{Cr(III)-OH-CA}]^-$ .

#### 2.4.3 Impacts of ionic strength

The impacts of ionic strength on adsorption can be used to determine the complexation mechanism between contaminants and porous media (Wu et al. 2010). As depicted in Fig. 8a, the Cr(III)-CA adsorption process fits well with both Freundlich and Langmuir models. With the increase in  $\text{Na}^+$  ionic strength in solutions from 0.001 M to 0.1 M, the adsorption capacity of Cr(III)-CA in silts increased marginally from 131.5  $\mu\text{g}/\text{g}$  to 138.1  $\mu\text{g}/\text{g}$ . This suggests that the enhancement of ionic strength has a negligible effect on Cr(III)-CA adsorption. Further analysis of the impacts of various coexisting cations on Cr(III)-CA adsorption in silts (Fig. 8b) revealed that coexisting  $\text{K}^+$ ,  $\text{Ca}^{2+}$ , and  $\text{Mg}^{2+}$  of varying strengths exhibited minor differences in their effects. Hence, these coexisting cations are unlikely to undergo ion exchange with Cr(III)-CA. The adsorption process, primarily governed by inner-sphere complexation, displayed minimal variation with an increase in ionic strength (Marsac et al. 2016; Cooper et al. 2009). This, as well as the desorption characteristics of

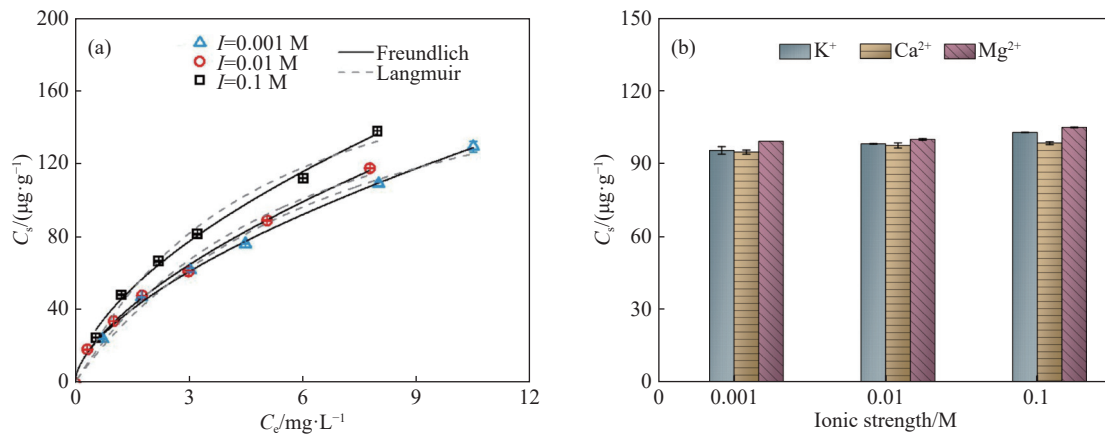


**Fig. 8** Effect of ionic strength and cations on the adsorption of Cr(III)-CA by silts (a: Ionic strength; b: Different cations)

Cr(III)-CA on porous media (Fig. 5), further demonstrates that the inner-sphere complexation predominates in Cr(III)-CA adsorption on porous media.

**2.4.4 Impacts of iron-aluminum oxides**

Iron-aluminum oxides, with their large SSAs and numerous active sites on their surfaces, serve as predominant sites for inner-sphere complexation between porous media and contaminants. As shown in Fig. 9, the adsorption capacity of Cr(III)-CA in both silts and fine sands significantly increased with the quantity of iron-aluminum oxides. With the iron-aluminum oxide content reaching 10 wt% in the porous media, Cr(III)-CA in solutions was nearly completely adsorbed and removed. The free carboxyl and hydroxyl groups in Cr(III)-CA readily undergo inner-sphere complexation with iron-aluminum oxides, forming robust complexes that are minimally affected by external environmental factors. Given the irreversible nature of the adsorption process of Cr(III)-CA and its minimal sensitivity to ionic strength,

inner-sphere complexation likely occurs between iron-aluminum oxides on porous media and Cr(III)-CA (Liu et al. 2011; Martin et al. 2015).

**3 Conclusions and recommendations**

The coordination of Cr(III) with CA results in the formation of stable and soluble Cr(III)-CA complexes. Under similar environmental conditions, the adsorption capacities of Cr(III)-CA in both silts and fine sands decrease by about one order of magnitude compared to those of Cr(III) ions. Additionally, the adsorption affinity of porous media for Cr(III)-CA of varying valencies decreases in the order of [Cr(III)-H-CA]<sup>+</sup>, [Cr(III)-CA]<sup>±</sup>, and [Cr(III)-OH-CA]<sup>-</sup>.

The adsorption processes of Cr(III)-CA in both silts and fine sands can be well fitted using both the Langmuir isotherm adsorption model and the pseudo-second-order kinetic equation. Notably, the adsorption rate and equilibrium adsorption capacity of Cr(III)-CA in silts are significantly higher than those observed in fine sands. These findings suggest that the adsorption of Cr(III)-CA is primarily affected by variations in the content of clay minerals and iron-aluminum oxides in porous media.

pH plays a crucial role in affecting the adsorption process of Cr(III)-CA by altering its form and the surface charges of porous media. The mechanisms governing the adsorption of Cr(III)-CA on porous media include cation exchange, electrostatic adsorption, and inner-sphere complexation. Under neutral pH conditions, the adsorption process of Cr(III)-CA on porous media is irreversible and minimally influenced by ionic strength, indicating that inner-sphere complexation acts as the dominant adsorption mechanism.

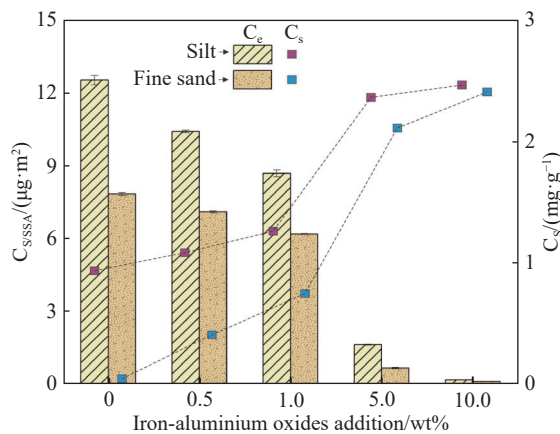


**Fig. 9** Effect of iron-aluminum oxides on the adsorption of Cr(III)-CA

This study focused solely on the representative Cr(III)-CA, which is prevalent in natural environments and leather production processes. However, in real-world environments, Cr(III)-organic complexes may exhibit more intricate behaviors and diverse forms. Moreover, microbial processes could potentially impact their migration and transformation dynamics. Therefore, it is recommended that future research endeavors focus on directly extracting Cr(III)-organic complexes from contaminated soils. This approach would yield results that serve as a more valuable practical guide for similar studies.

## Acknowledgements

This study was financially supported jointly by Natural Science Foundation of Fujian Province of China (NO. 2023J01227), Natural Science Foundation of Hebei Province (NO. D2020504003), Key Laboratory of Groundwater Remediation of Hebei Province and China Geological Survey (NO. SK202303).

## References

- Cooper E, Vasudevan D. 2009. Hydroxynaphthoic acid isomer sorption onto goethite. *Journal of Colloid and Interface Science*, 333(1): 85–96. DOI: [10.1016/j.jcis.2009.02.023](https://doi.org/10.1016/j.jcis.2009.02.023).
- Cao XH, Guo J, Mao JD, et al. 2011. Adsorption and mobility of Cr(III)-organic acid complexes in soils. *Journal of Hazardous Materials*, 192(3): 1533–1548. DOI: [10.1016/j.jhazmat.2011.06.076](https://doi.org/10.1016/j.jhazmat.2011.06.076).
- Chiavola A, Amato E, Boni M. 2019. Comparison of different iron oxide adsorbents for combined arsenic, vanadium and fluoride removal from drinking water. *International Journal of Environmental Science & Technology*, 16(10): 6053–6064. DOI: [10.1007/s13762-019-02316-4](https://doi.org/10.1007/s13762-019-02316-4).
- Dai RN, Liu J, Yu CY, et al. 2009. A comparative study of oxidation of Cr(III) in aqueous ions, complex ions and insoluble compounds by manganese-bearing mineral (birnessite). *Chemosphere*, 76(4): 536–541. DOI: [10.1016/j.chemosphere.2009.03.009](https://doi.org/10.1016/j.chemosphere.2009.03.009).
- Gustafsson J, Persson I, Oromieh A, et al. 2014. Chromium(III) complexation to natural organic matter: Mechanisms and modeling. *Environment Science & Technology*, 48: 1753–1761. DOI: [10.1021/es404557e](https://doi.org/10.1021/es404557e).
- Gérard F. 2016. Clay minerals, iron/aluminum oxides, and their contribution to phosphate sorption in soils—A myth revisited. *Geoderma*, 262(15): 213–226. DOI: [10.1016/j.geoderma.2015.08.036](https://doi.org/10.1016/j.geoderma.2015.08.036).
- Guo HM, Chen Y, Hu HY, et al. 2020. High hexavalent chromium concentration in groundwater from a deep aquifer in the baiyangdian basin of the north China plain. *Environmental Science & Technology*, 54(16): 10068–10077. DOI: [10.1021/acs.est.0c02357](https://doi.org/10.1021/acs.est.0c02357).
- Hizal J, Apak R. 2013. Kinetic investigation and surface complexation modeling of Cd(II) adsorption onto feldspar. *Fresenius Environmental Bulletin*, 22(3): 766–771. DOI: [10.1021/ma00183a057](https://doi.org/10.1021/ma00183a057).
- Hao YY, Ma HR, Wang Q, et al. 2022. Complexation behavior and removal of organic-Cr(III) complexes from the environment: A review. *Ecotoxicology and Environmental Safety*, 240: 113676. DOI: [10.1016/j.ecoenv.2022.113676](https://doi.org/10.1016/j.ecoenv.2022.113676).
- James B, Bartlett R. 1983. Behavior of chromium in soils: V. Fate of organically complexed Cr(III) added to soil. *Journal of Environmental Quality*, 12(2): 169–172. DOI: [10.2134/jeq1983.00472425001200020003x](https://doi.org/10.2134/jeq1983.00472425001200020003x).
- Kah M, Sigmund G, Xiao F, et al. 2017. Sorption of ionizable and ionic organic compounds to biochar, activated carbon and other carbonaceous materials. *Water Research*, 124: 673–692. DOI: [10.1016/j.watres.2017.07.070](https://doi.org/10.1016/j.watres.2017.07.070).
- Kanagaraj G, Elango L. 2019. Chromium and fluoride contamination in groundwater around leather tanning industries in southern India: implications from stable isotopic ratio Delta Cr-53/Delta Cr-52, geochemical and geostatistical modelling. *Chemosphere*, 220: 943–953. DOI: [10.1016/j.chemosphere.2018.12.105](https://doi.org/10.1016/j.chemosphere.2018.12.105).
- Kong XK, Li CH, Wang P, et al. 2019. Soil pollution characteristics and microbial responses in a vertical profile with long-term tannery sludge contamination in Hebei, China. *International Journal of Environmental Research and Public Health*, 16(4): 563–570. DOI: [10.3390/ijerph16040563](https://doi.org/10.3390/ijerph16040563).

- 3390/ijerph16040563.
- Kong XK, Wang Y, Ma LS, et al. 2020. Leaching behaviors of chromium (III) and ammonium-nitrogen from a tannery sludge in north China: Comparison of batch and column investigations. *International Journal of Environmental Research and Public Health*, 17: 6003. DOI: [10.3390/ijerph17166003](https://doi.org/10.3390/ijerph17166003).
- Luo Z, Wadhawan A, Bouwer E. 2010. Sorption behavior of nine chromium (III) organic complexes in soil. *International Journal of Environmental Science and Technology*, 7(1): 1–10. DOI: [10.1007/BF03326111](https://doi.org/10.1007/BF03326111).
- Li F. 2009. Synthesis, characterization and preliminary application of several organic chromium complexes. MS thesis, Zhenjiang: Jiangsu University: 23. (in Chinese)
- Li H, Han ZT, Deng Q, et al. 2023. Assessing the effectiveness of nanoscale zero-valent iron particles produced by green tea for Cr(VI)-contaminated groundwater remediation. *Journal of Groundwater Science and Engineering*, 11(1): 55–67. DOI: [10.26599/JGSE.2023.9280006](https://doi.org/10.26599/JGSE.2023.9280006).
- Liu W, Zhang J, Zhang C, et al. 2011. Sorption of norfloxacin by lotus stalk-based activated carbon and iron-doped activated alumina: Mechanisms, isotherms and kinetics. *Chemical Engineering Journal*, 171(2): 431–438. DOI: [10.1016/j.cej.2011.03.099](https://doi.org/10.1016/j.cej.2011.03.099).
- Li BR, Liao P, Liu P, et al. 2022. Formation, aggregation and transport of NOM-Cr(III) colloids in aquatic environments. *Environmental Science-Nano*, 9(3): 1133–1145. DOI: [10.1039/d1en00861g](https://doi.org/10.1039/d1en00861g).
- Martin S, Shchukarev A, Hanna K, et al. 2015. Kinetics and mechanisms of ciprofloxacin oxidation on hematite surfaces. *Environment Science & Technology*, 49(20): 12197–12205. DOI: [10.1021/acs.est.5b02851](https://doi.org/10.1021/acs.est.5b02851).
- Merdoud O, Cameselle C, Boulakradeche MO, et al. 2016. Removal of heavy metals from contaminated soil by electro dialytic remediation enhanced with organic acids. *Environmental Science-Processes & Impacts*, 18(11): 1440–1448. DOI: [10.1039/c6em00380j](https://doi.org/10.1039/c6em00380j).
- Marsac R, Martin S, Boily J, et al. 2016. Oxolinic acid binding at goethite and akaganeite surfaces: Experimental study and modeling. *Environmental Science & Technology*, 50(2): 660–678. DOI: [10.1021/acs.est.5b04940](https://doi.org/10.1021/acs.est.5b04940).
- Ma H, Zhou J, Hua L, et al. 2017. Chromium recovery from tannery sludge by bioleaching and its reuse in tanning process. *Journal of Cleaner Production*, 142(8): 2752–2760. DOI: [10.1016/j.jclepro.2016.10.193](https://doi.org/10.1016/j.jclepro.2016.10.193).
- Manoj S, RamyaPriya R, Elango L. 2021. Long-term exposure to chromium contaminated waters and the associated human health risk in a highly contaminated industrialized region. *Environmental Science and Pollution Research*, 28(4): 4276–4288. DOI: [10.1007/s11356-020-10762-8](https://doi.org/10.1007/s11356-020-10762-8).
- Puzon G, Tokala R, Zhang H, et al. 2008. Mobility and recalcitrance of organo-chromium(III) complexes. *Chemosphere*, 70(11): 2054–2059. DOI: [10.1016/j.chemosphere.2007.09.010](https://doi.org/10.1016/j.chemosphere.2007.09.010).
- Pantazopoulou E, Zouboulis A. et al. 2017. Chemical toxicity and ecotoxicity evaluation of tannery sludge stabilized with ladle furnace slag. *Journal of Environmental Management*, 216: 257–262. DOI: [10.1016/j.jenvman.2017.03.077](https://doi.org/10.1016/j.jenvman.2017.03.077).
- Qiang TT, Bu QQ, Ren LF, et al. 2014. Adsorption behaviors of Cr(III) on carboxylated collagen fiber. *Journal of Applied Polymer Science*, 131(11): 2928–2935. DOI: [10.1002/app.40285](https://doi.org/10.1002/app.40285).
- Reijonen I, Hartikainen H. 2016. Oxidation mechanisms and chemical bioavailability of chromium in agricultural soil-pH as the master variable. *Applied Geochemistry*, 74: 84–93. DOI: [10.1016/j.apgeochem.2016.08.017](https://doi.org/10.1016/j.apgeochem.2016.08.017).
- Schwab A, He Y, Banks M. 2005. The influence of organic ligands on the retention of lead in soil. *Chemosphere*, 61(6): 856–866. DOI: [10.1016/j.chemosphere.2005.04.098](https://doi.org/10.1016/j.chemosphere.2005.04.098).
- Sethunathan N, Megharaj M, Smith L, et al. 2005. Microbial role in the failure of natural attenuation of Chromium(VI) in long-term tannery waste contaminated soil. *Agriculture, Ecosystems & Environment*, 105(4): 657–661. DOI: [10.1016/j.agee.2004.08.008](https://doi.org/10.1016/j.agee.2004.08.008).
- Shashirekha V, Sridharan MR, Swamy, M. 2015. Biochemical response of cyanobacterial species to trivalent chromium stress. *Algal Research*, 12: 421–430. DOI: [10.1016/j.algal.2015.10.003](https://doi.org/10.1016/j.algal.2015.10.003).
- Shi GW, Li YS, Liu YC, et al. 2023. Predicting the

- speciation of ionizable antibiotic ciprofloxacin by biochars with varying carbonization degrees. *RSC Advances*, 13: 9892–9902. DOI: [10.1039/d3ra00122a](https://doi.org/10.1039/d3ra00122a).
- Tripathi S, Chaurasia S. 2020. Detection of chromium in surface and groundwater and its bio-absorption using bio-wastes and vermiculite. *Engineering Science and Technology-an International Journal-Jestech*, 23(5): 1153–1161. DOI: [10.1016/j.jestch.2019.12.002](https://doi.org/10.1016/j.jestch.2019.12.002).
- Marsac R, Martin S, Boily J, et al. 2010. Oxolinic acid binding at goethite and akaganeite surfaces: Experimental study and modeling. *Environmental Science & Technology*, 29(6): 997–1003. (in Chinese)
- Wang CL, Liu CL, Pang YJ, et al. 2013. Adsorption behavior of hexavalent chromium in vadose zone. *Journal of Groundwater Science and Engineering*, 1(3): 83–88. DOI: [10.26599/JGSE.2013.9280034](https://doi.org/10.26599/JGSE.2013.9280034).
- Wang DD, He SY, Shan C, et al. 2016. Chromium speciation in tannery effluent after alkaline precipitation: Isolation and characterization. *Journal of Hazardous Materials*, 316: 169–177. DOI: [10.1016/j.jhazmat.2016.05.021](https://doi.org/10.1016/j.jhazmat.2016.05.021).
- Wang P, Kong XK, Ma LS, et al. 2022. Metal(loid)s removal by zeolite-supported iron particles from mine contaminated groundwater: Performance and mechanistic insights. *Environmental Pollution*, 313: 120155. DOI: [10.1016/j.envpol.2022.120155](https://doi.org/10.1016/j.envpol.2022.120155).
- Yang SY, Cheng Y, Zou HT, et al. 2022. Synergistic roles of montmorillonite and organic matter in reducing bioavailable state of chromium in tannery sludge. *Environmental Science and Pollution Research*, 29(58): 87298–87309. DOI: [10.1007/s11356-022-21897-1](https://doi.org/10.1007/s11356-022-21897-1).
- Zeng J, Gou M, Tang YQ, et al. 2016. Effective bioleaching of chromium in tannery sludge with an enriched sulfur-oxidizing bacterial community. *Bioresource Technology*, 218: 859–866. DOI: [10.1016/j.biortech.2016.07.051](https://doi.org/10.1016/j.biortech.2016.07.051).
- Zhang W, Chen Z, Han ZT, et al. 2022. Adsorption characteristics of Pb(II) and Cd(II) in water bodies onto biochars derived from 7-ACA fermented residue. *Safety and Environmental Engineering*, 29(4): 212–220. (in Chinese) DOI: [10.13578/i.cnki.issn.1671-1556.20210694](https://doi.org/10.13578/i.cnki.issn.1671-1556.20210694).